459123

Evidence of Lunar Phase Influence on Global Surface Air Temperatures

E. Anyamba[1], and J. Susskind[2]

[1] General Sciences Corporation, NASA GSFC

[2] NASA Goddard Space Flight Center, Code 910.4, Greenbelt, MD 20771

Abstract

Intraseasonal oscillations appearing in a newly available 20-year record of satellite-derived surface air temperature are composited with respect to the lunar phase. Polar regions exhibit strong lunar phase modulation with higher temperatures occuring near full moon and lower temperatures at new moon, in agreement with previous studies. The polar response to the apparent lunar forcing is shown to be most robust in the winter months when solar influence is minimum. In addition, the response appears to be influenced by ENSO events. The highest mean temperature range between full moon and new moon in the polar region between 60° and 90 ° latitude was recorded in 1983, 1986/87, and 1990/91. Although the largest lunar phase signal is in the polar regions, there is a tendency for meridional equatorward progression of anomalies in both hemispheres so that the warming in the tropics accurs at the time of the new moon.

1. Introduction

Over the last four decades a number of studies have identified significant lunar phase signal in precipitation (Bradley et al, 1962, Adderley and Bowen, 1962, Brier and Bradley, 1964, Hanson et al, 1987), thunderstorm frequency (Lethbridge, 1970), and in sunshine observations (Lund, 1965). A number of these studies have been reviewed by Markson (1971). More recently, lunar phase modulation has been detected in satellite-derived global lower tropospheric (lowest 6 km) temperatures (Balling and Cerveny, 1995a,b, Shaffer et al, 1997). The relationship between the global temperatures and lunar phase is such that the Earth is warmer by 0.02 degrees at the time of full moon compared to the time of the new moon.

A number of possible mechanisms have been proposed to explain this modulation. They include: (i) the effect of lunar tidal forces on atmospheric circulation patterns (Hanson et al, 1987, Nicholls and Pielke, 1993, 1994), (ii) direct effect of emitted and reflected radiation from the lunar surface (Balling and Cerveny, 1995), and (iii) changes in incoming solar radiation due to barycentric motion of the Earth and moon which places the Earth closer to the sun at the time of the full moon than it is on average (Dyre, 1995, Voorhies, 1995).

In the present study we use a newly available 20-year record of satellite-derived daily global surface air temperature to show further evidence of the lunar phase modulation reported by Balling and Cerveny (1995a,b) and Shaffer et al (1997). Further, we show that this modulation is more dominant during the winter months of either hemisphere. Moreover, a preliminary investigation of the year-to-year variability of this relationship has revealed what appears to be an ENSO influence on the amplitude of the lunar phase signal: the range in polar temperature difference between full moon and new moon is highest during the El Ninos of 1993, 1986/87, and 1990/91.

2. Data

The Goddard TIROS Operational Vertical Sounder (TOVS) surface air temperature is part of a set of geophysical fields derived from radiances measured by the High Resolution Infrared Sounder2 (HIRS2) and Microwave Sounding Unit (MSU) instruments on board the NOAA polar orbiting satellites. Although these instruments are primarily designed for atmospheric sounding, the Path A interactive forecast-retrieval-analysis system used to retrieve the parameters also produces estimates of surface air temperature and specific humidity in the lowest 50 meters of the atmosphere (Susskind et al, 1997). The parameters are obtained by using the shape of the model forecast field in the boundary layer and the TOVS measurements in HIRS2 4.57 and 4.52 channels which are sensitive to temperatures near the Earth's surface. This surface air temperature compares well with in-situ observations (Anyamba and Susskind, 1997).

Over the 20-year period, 1979-1998, the TOVS data are available four times a day (0130, 0730, 1330, 1930 LT) in 1981-1983 and 1989-1998, and twice daily in 1979-1981, and 1984-1988. In this study we used a blend of the 1330 and 1930 LT observations in 1989-1998, 0130 and 1330 LT in 1979 and 1984-1987, and, a blend of 0730 and 1930 LT in 1987-1988. The blending fills data gaps in one orbit with values from the second orbit. Any remaining data gaps were filled with weighted averages from the surrounding eight grid points. Dates of the full moon for 1979-1998 were obtatined from Ray Sterner's web site at http://fermi.jhuapl.edu/slr/amastro/tools/fullmoons.txt.

3. Analysis

A preliminary spectral analysis of the 20-year daily global mean surface air temperature revealed a series of statistically significant spectral peaks in the intraseasonal range of 20-50 days (Figure 1). Our main task is to determine the relationship between these variations and the lunar phase. In order to isolate the intraseasonal variations, the time series for each year at every grid point were band-pass filtered by a Fourier based filter that removed periods shorter than 7 days and longer than 60 days. The routine is described in Press et al (1986, pages 495-497). The

resulting daily anomalies were then composited relative to the date of the full moon for each of the 245 lunar months in the entire 20-year period. The results presented below are based on the average of these 245 lunar months.

4.Results

Seasonal dependence of the lunar phase influence

Figure 2 (a) shows the evolution of zonal mean intraseasonal anomalies relative to the phase of the full moon. The anomalies are averages over 245 lunar cycles in the 20-year period. This figure shows a clear stratification of high latitude anomalies relative to the phase of the lunar cycle. Positive anomalies in excess of 0.3°C occur several days prior to the full moon, while negative anomalies occur around the new moon. This result is in excellent agreement with the findings of Shaffer et al (1997) who used MSU2 data for the period 1979-1996.

One of the mechanisms suggested for the warmer temperatures at the time of the full moon is direct heating by emitted and reflected radiation from the lunar surface. To address this possibility, we divided the composites into two sets corresponding to the northern hemisphere (NH) winter (October-March), and southern hemisphere (SH) winter (April-September). These seasons correspond to the time of the year when at least some part of the respective polar regions receives no sunshine. (Fig. 7.16, Wallace and Hobbs, 1977). Radiation from the lunar surface is expected to play a relatively major role in modulating the polar temperatures in winter compared to the summer season. Figures 2 (b) and (c) show the seasonal composites for the NH winter and SH winter, respectively. Indeed the signals are stronger and the lunar phase relationship better defined in the winter hemisphere. In particular, in the region between 60° and 90° latitude, the zonal mean temperature difference between full moon and new moon exceeds 0.8°C. Shaffer et al reported values exceeding 0.55°C on annual mean basis. An interesting feature to note especially in the NH is the tendency for the middle latitudes (40°-60°N) to be out of phase with the polar regions. The anomalies also have a slight equatorward propagation so that the positive

anomalies in the tropics (about 0.02) occur around the new moon period. This differential warming at different latitudes was also noted by Shaffer et al (1997).

Year-to-year variability of the lunar phase signal

In order to determine the statistical significance and reproducibility of the relationship in Figure 2, we computed an index that is a measure of the amplitude or strength of the lunar phase signal. This index is computed as the 7-day area-mean temperature anomaly in the latitude band 60°-90° at full moon (-/+ 3 days) minus the corresponding anomaly at new moon (-/+ 3 days). This index was computed for each lunar month, then averaged to form NH winter and SH winter averages for each year. Winter 1979 corresponds to October 1979 to March 1980. Figure 3 shows the 20-year timeseries of the NH winter (thick line) and SH winter (thin line). The 20-year mean values of these indices are 0.24°C and 0.36°C, with standard deviations of 0.5° and 0.6°C for the NH winter and SH winter, respectively.

To test the statistical significance of the indices, a set of monthly composites determined in the same manner as the lunar phase composites were generated using different days of the month (the 1st, 9th, 17th and 25th) as the key days in place of the full moon dates. Indices defined as the 60°-90° area-averaged anomaly at the key date (-/+ 3 days) minus the anomaly 14 days later (-/+ 3 days) were then used in a two-sample Student's t-test to determine the significance of the indices in Figure 3. Both indices are highly significant at 0.01 significance level. Global mean indices (not shown) were also computed. The global mean temperature difference between full moon and new moon was 0.032 in SH winter and only 0.003 in NH winter, with an annual average of 0.017. This value is in good agreement with the value of 0.02 reported by Balling and Cerveny (1995). The global mean during SH winter is highly significant at 0.01 level, while the NH winter value is only marginally significant at 0.10 level. This is probably due to the stronger synoptic scale systems in the NH winter which mask weak global scale signals.

The indices in Figure 3, are positive on average, confirming the result that the polar regions

are warmer at full moon compared to new moon. However there is marked interannual variability. The largest amplitudes exceeding one standard deviation for both hemispheres occurred during 1983, 1986/87, and 1990/91 (El Nino years). The SH winter amplitude was also high in 1993 and 1996. On the other hand 1989 (La Nina year) had the lowest value. Zonal mean anomalies were averaged over the years 1983, 84, 86,87, 90, 91, 93, and 96 for SH winter, and 1981, 83, 87, 90, and 91 for NH winter. The prominent feature (not shown) was not only a much higher temperature range (about 2°C) between full moon and new moon, but also a marked equatorward progression of anomalies. On the other hand, the average of 1989 and 1992 showed a slight warming in the midlatitudes at the full moon, which then progressed poleward. This apparent ENSO-related modulation is an interesting finding in the present study and would imply that even though there may be external lunar related modulation of surface air temperature, its effect may be dependent on the prevailing conditions determined by other signals in the Earth's climate system. In Figure 4, we present an example of the actual timeseries of zonal mean anomalies for April 1986 to March 1987. We note that although the anomalies are strongest in the polar regions (range of about 6°C), they extend into the tropics where the range is about 0.8°C. There is a tendency for equatorward progression of anomalies so that the equatorial zone lags the polar regions by about two weeks.

5. Discussion

Intraseasonal oscillations have been studied extensively since the discovery of the tropical component by Madden and Julian (1972). Though the oscillations are known to be global, detailed studies of the polar regions have been hampered by lack of reliable daily observations. The TOVS data used here are not only available daily on a 1° by 1° grid, but also contain realistic intraseasonal signals (Anyamba et al, 2000).

Balling and Cerveny (1995a,b) and Shaffer et al (1997) were the first to link the oscillations in

the polar regions to lunar-related forcing. In the present study we present further evidence of this influence using the newly available satellite-derived surface air temperature data set. Unlike, the MSU2 product used in the previous study, the TOVS product is more representative of conditions near the Earth's surface. Nonetheless, the results presented here are in excellent agreement with the previous findings. We have further shown that the lunar phase signal in the polar regions is more robust during the winter months when radiation from the moon is expected to have a more significant effect on polar temperatures. This finding supports direct radiation from the lunar surface as being the cause of the warmer temperatures experienced at full moon. During the winter months, the 20-year mean zonally-averaged temperature difference between full moon and new moon is 0.24° in the northern polar regions and 0.36° in the southern polar regions. The corresponding seasonal range between winter and summer is about 30° C in the NH and 20°C is SH. The the lunar phase signal is thus only 0.8 and 1.8 percent of the respective seasonal cycle in the NH, and SH polar regions. Nonetheless, it is highly significant and requires further study as a likely external forcing mechanism on the intraseasonal time scales.

A further finding in this study is the apparent modulation of the lunar phase signal by ENSO events. The temperature range between full moon and new moon was largest during the El Nino events of 1983, 1986/87, and 1990/91, but not the recent 1997/98 event. During these years there was marked equatorward progression of the anomalies during the lunar month so that the tropics lagged the polar regions by about two weeks. ENSO events are known to modulate polar climates (e.g. Gloersen, 1995) and it is likely that the response of the polar regions to lunar forcing depends on the prevailing conditions, such as cloud cover and precipitation which are themselves modulated by ENSO. On the other hand, intraseasonal variations are believed to play a role in triggering El Nino onset (Lau and Chan, 1986). Further investigations using the now available data sets should shed some light on the possibility of lunar-related mechanisms as being the primary forcing for the global intraseasonal oscillations. Understanding of the nature of

interaction between these oscillations and the ENSO phenomenon would also contribute toward improvement of short-term climate prediction.

6. Acknowledgements

The authors wish to thank Paul Piraino, Jeff Whitting and Lena Iredell for availing the daily surface air temperature data. Discussions with Christopher Barnett and John Blaisdell are also appreciated. This work was partially funded by the NASA OSS Solar Influences on Global Change Research and Analysis Program, RTOP 406-04-00-01.

7. References

Adderley, E.E. and E.G. Bowen,1962: Lunar component in precipitation data. *Science, 137*, 749-750.

Anyamba, E., E. Williams, J. Susskind, A. Fraser-Smith, and M. Fullekrug, 2000: The manifestation of the Madden-Julian oscillation in global deep convection and in Schumann resonance intensity. *J. Atmos. Sci., 57*, 1029-1044.

Anyamba, E. and J. Susskind, 1997: A comparison of TOVS ocean skin and surface air temperatures with other data sets. *J. Geophys. Res., 103*, 10,489-10,511.

Balling, R.C., Jr. and R.S. Cerveny, 1995a: Influence of lunar phase on daily global temperatures. *Science, 267*, 1481-1483.

Balling, R.C., Jr. and R.S. Cerveny, 1995b: Impact of lunar phase on the timing of global and latitudinal tropospheric temperature maxima. *Geophys. Res. Lett., 22*, 3199-3201.

Bradley, D.A., M.A. Woodbury and G.W. Brier, 1962: Lunar synodical period and widespread precipitation. *Science, 137*,748-749.

Dyre, J.C., 1995: Lunar phase influence on global temperatures, *Science, 269*, 1284-1285.

Brier, G.W. and D.A. Bradley, 1964: The lunar synodical period and precipitation in the United States. *J. Atmos. Sci., 21*, 386-395.

Gloersen, P., 1995: Modulationn of hemispheric sea-ice cover by ENSO events. *Nature, 373*, 503-506.

Hanson, K., G.A. Maul and W. McLeish, 1987: Precipitation and the lunar synodic cycle: Phase progression across the the United States. *J. Clim. Appl. Meteor., 26*, 1358-1362.

Lau, K.M. and P.H. Chan, 1998: The 40-50 day oscillation and the El Nino/Southern Oscillation: A new perspective. *Bull. Amer. Met. Soc., 67*, 533-534.

Lethbridge, M.D., 1970: Relationship between thunderstorm frequency and lunar phase and declination. *J. Geophys. Res., 75*, 5149-5154.

Lund, I.A., 1965: Indications of a lunar synodical period in United States observations of sunshine. *J. Atmos. Scie.,22*, 24-39.

Markson, R., 1971: Considerations regarding solar and lunar modulation of geophysical parameters, atmospheric electricity and thunderstorms. *Pure Appl. Geophys., 84*, 161-200.

Nicholls, M.E., and R.A. Pielke, 1993: Thermal compression waves, I: Total-energy transfer, *Q. J. R. Meteor. Soc., 120*, 305-332.

Nicholls, M.E., and R.A. Pielke, 1994: Thermal compression waves, II: Mass adjustment and vertical transfer of total energy. *Q. J. R. Meteor. Soc., 120*, 333-359.

Press, W.H., B.P. Flannery, S.A. Teukolsky and W.T. Vetterling, 1986: *Numerical Recipes, the art of scientific computing.* Cambridge University Press, 818pp.

Shaffer, J.A., R.S. Cerveny and R.C. Balling, Jr., 1997: Polar temperature sensitivity to lunar forcing? *Geophys. Res. Lett.,24*, 29-32.

Susskind, P. Piraino, L. Rokke, L. Iredell and A. Mehta, 1997: Characteristics of the TOVS Pathfinder Path A data set. *Bull. Amer. Met. Soc., 78*, 1449-1472.

Voorhies, C.V., 1995: Lunar phase influence on global temperatures, *Science, 269*, 1285.

Figure Captions

Figure 1: Power spectrum of 20-year record of daily global mean surface air temperature (K^2.day). The thick curve is the power spectral density normalized by the variance, thin curve is the estimated red noise, and the dotted curve is the 99% confidence level.

Figure 2: 20-year mean zonally averaged intraseasonal anomalies composited with respect to the date of the full moon: (a) annual mean, (b) October-March (NH winter), (c) April-September (SH winter).

Figure 3: Timeseries of an index of the temperature range between full moon and new moon for NH winter (thick curve) and SH winter (thin curve).

Figure 4: Timeseries of zonally-averaged intraseasonal temperature anomalies (°C) from April 1986 to March 1987.

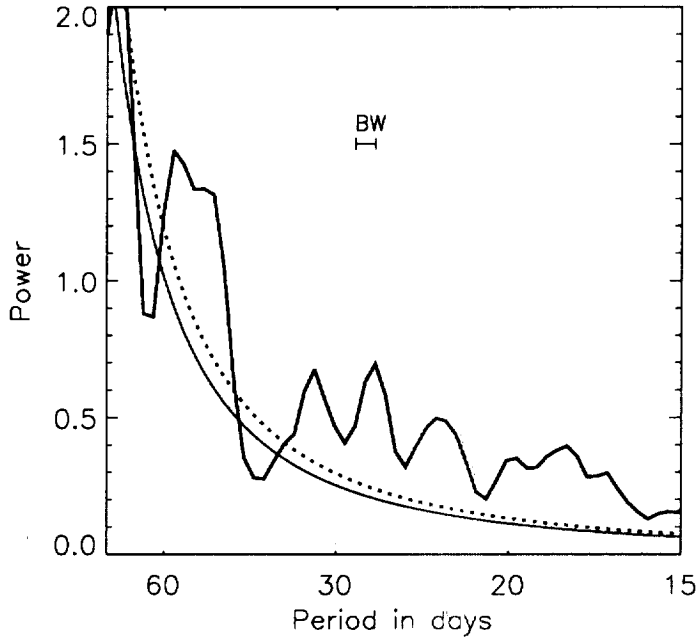
2.0
1.5
1.0
0.5
0.0
Power
BW
60
30
20
15
Period in days

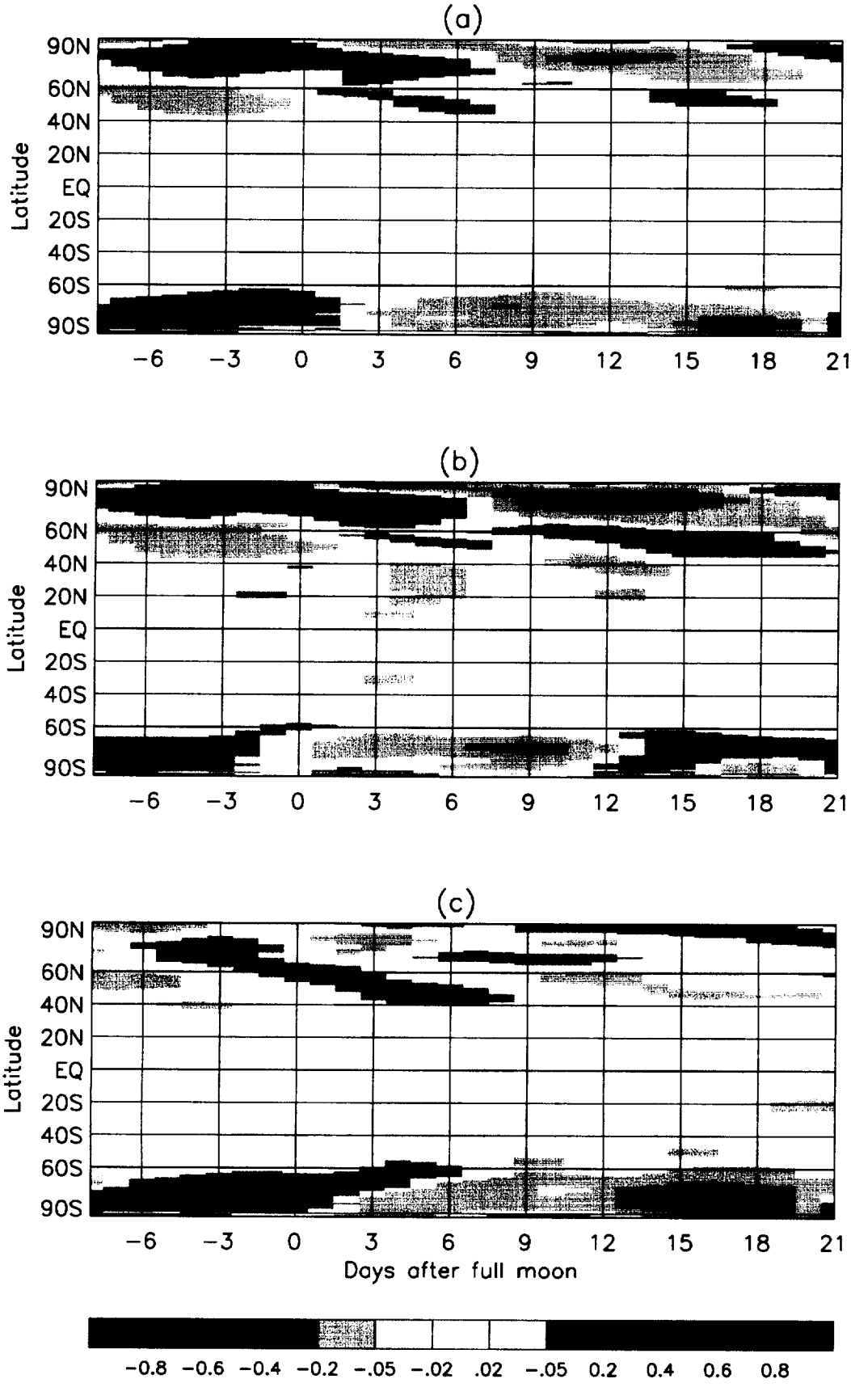
(a)
90N
60N
40N
20N
EQ
20S
40S
60S
90S
Latitude
−6 −3 0 3 6 9 12 15 18 21
(b)
90N
60N
40N
20N
EQ
20S
40S
60S
90S
Latitude
−6 −3 0 3 6 9 12 15 18 21
(c)
90N
60N
40N
20N
EQ
20S
40S
60S
90S
Latitude
−6 −3 0 3 6 9 12 15 18 21
Days after full moon
−0.8 −0.6 −0.4 −0.2 −.05 −.02 .02 −.05 0.2 0.4 0.6 0.8

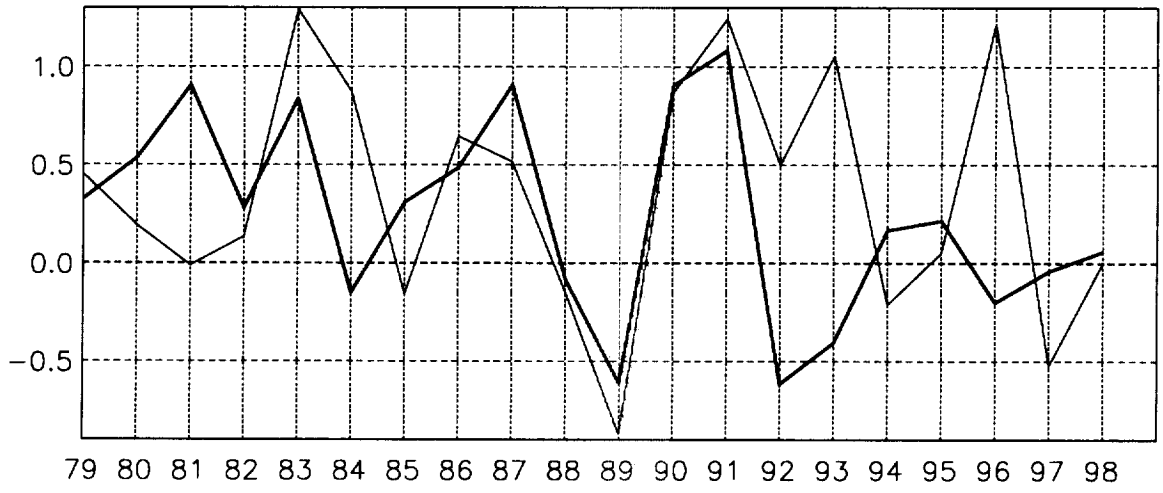
1.0
0.5
0.0
−0.5
79 80 81 82 83 84 85 86 87 88 89 90 91 92 93 94 95 96 97 98

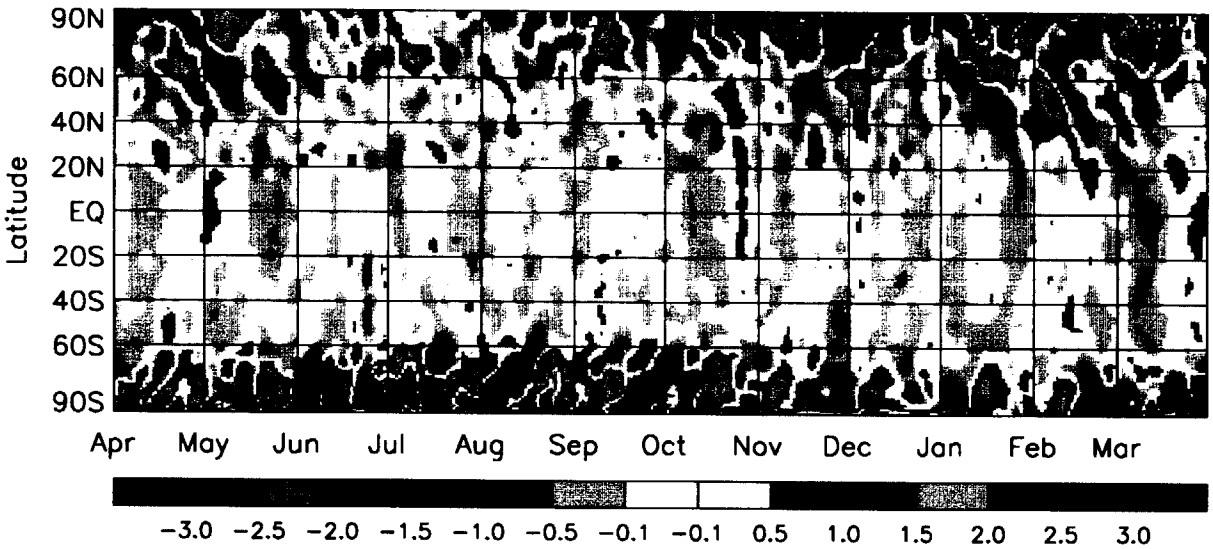
90N
60N
40N
20N
EQ
20S
40S
60S
90S
Latitude
Apr
May
Jun
Jul
Aug
Sep
Oct
Nov
Dec
Jan
Feb
Mar
−3.0
−2.5
−2.0
−1.5
−1.0
−0.5
−0.1
−0.1
0.5
1.0
1.5
2.0
2.5
3.0